AFRL-RX-WP-JA-2017-0149

SPATIAL TUNING OF A RF FREQUENCY SELECTIVE SURFACE THROUGH ORIGAMI (POSTPRINT)

George Bazzan
UES

Philip R. Buskohl, Michael F. Durstock, James J. Joo, Gregory W. Reich, and Richard A. Vaia
AFRL/RX

Kazuko Fuchi
Wright State University

18 April 2016
Interim Report

(STINFO COPY)

AIR FORCE RESEARCH LABORATORY
MATERIALS AND MANUFACTURING DIRECTORATE
WRIGHT-PATTERSON AIR FORCE BASE, OH 45433-7750
AIR FORCE MATERIEL COMMAND
UNITED STATES AIR FORCE

REPORT DOCUMENTATION PAGE

Form Approved
OMB No. 0704-0188

1. REPORT DATE *(DD-MM-YY)*	2. REPORT TYPE	3. DATES COVERED *(From - To)*
18 April 2016	Interim	10 March 2014 – 18 March 2016

4. TITLE AND SUBTITLE
SPATIAL TUNING OF A RF FREQUENCY SELECTIVE SURFACE THROUGH ORIGAMI (POSTPRINT)

5a. CONTRACT NUMBER
FA8650-14-C-5003

5b. GRANT NUMBER

5c. PROGRAM ELEMENT NUMBER
65502F

6. AUTHOR(S)
1) George Bazzan – UES
2) Philip R. Buskohl, Michael F. Durstock, James J. Joo, Gregory W. Reich, and Richard A. Vaia - AFRL/RX
(continued on page 2)

5d. PROJECT NUMBER
3005

5e. TASK NUMBER

5f. WORK UNIT NUMBER
X0UY

7. PERFORMING ORGANIZATION NAME(S) AND ADDRESS(ES)
1) UES, Inc, 4401 Dayton Xenia Rd, Beavercreek, OH 45432
2) AFRL/RX Wright-Patterson AFB, OH 45433
(continued on page 2)

8. PERFORMING ORGANIZATION REPORT NUMBER

9. SPONSORING/MONITORING AGENCY NAME(S) AND ADDRESS(ES)
Air Force Research Laboratory
Materials and Manufacturing Directorate
Wright-Patterson Air Force Base, OH 45433-7750
Air Force Materiel Command
United States Air Force

10. SPONSORING/MONITORING AGENCY ACRONYM(S)
AFRL/RXAS

11. SPONSORING/MONITORING AGENCY REPORT NUMBER(S)
AFRL-RX-WP-JA-2017-0149

12. DISTRIBUTION/AVAILABILITY STATEMENT
Distribution Statement A. Approved for public release: distribution unlimited.

13. SUPPLEMENTARY NOTES
PA Case Number: 88ABW-2016-1963; Clearance Date: 18 Apr 2016. This document contains color. Journal article published in Proc. of SPIE 9844: Automatic Target Recognition XXV, Vol. 9844, 12 May 2016.
The final publication is available at http://dx.doi.org/10.1117/12.2224160

14. ABSTRACT *(Maximum 200 words)*
Origami devices have the ability to spatially reconfigure between 2D and 3D states through folding motions. The precise mapping of origami presents a novel method to spatially tune radio frequency (RF) devices, including adaptive antennas, sensors, reflectors, and frequency selective surfaces (FSSs). While conventional RF FSSs are designed based upon a planar distribution of conductive elements, this leaves the large design space of the out of plane dimension underutilized.
We investigated this design regime through the computational study of four FSS origami tessellations with conductive dipoles. The dipole patterns showed increased resonance shift with decreased separation distances, with the separation in the direction orthogonal to the dipole orientations having a more significant effect. The coupling mechanism between dipole neighbors were evaluated by comparing surface charge densities, which revealed the gain and loss of coupling as the dipoles moved in and out of alignment via folding. Collectively, these results provide a basis of origami FSS designs for experimental study and motivates the development of computational tools to systematically predict optimal folds.

15. SUBJECT TERMS
origami, frequency selective surface, tuning, radio frequency

16. SECURITY CLASSIFICATION OF:			17. LIMITATION OF ABSTRACT:	18. NUMBER OF PAGES	19a. NAME OF RESPONSIBLE PERSON (Monitor)
a. REPORT	b. ABSTRACT	c. THIS PAGE			Philip Buskohl
Unclassified	Unclassified	Unclassified	SAR	13	19b. TELEPHONE NUMBER *(Include Area Code)* (937) 255-9152

REPORT DOCUMENTATION PAGE Cont'd

6. AUTHOR(S)

3) Kazuko Fuchi - WSU

7. PERFORMING ORGANIZATION NAME(S) AND ADDRESS(ES)

3) Wright State Research Institute
4035 Colonel Glenn Hwy., Suite 200
Beavercreek, OH 45431

Spatial tuning of a RF frequency selective surface through origami

Kazuko Fuchi[b], Philip R. Buskohl*[a], Giorgio Bazzan[c], Michael F. Durstock[a], James J. Joo[a], Gregory W. Reich[a] and Richard A. Vaia[a]
[a]Air Force Research Laboratory, 2941 Hobson Way, Wright-Patterson AFB, OH 45433-7750;
[b]Wright State Research Institute, 4035 Colonel Glenn Hwy., Suite 200, Beavercreek, OH 45431;
[c]UES, Inc, 4401 Dayton Xenia Rd, Beavercreek, OH 45432

ABSTRACT

Origami devices have the ability to spatially reconfigure between 2D and 3D states through folding motions. The precise mapping of origami presents a novel method to spatially tune radio frequency (RF) devices, including adaptive antennas, sensors, reflectors, and frequency selective surfaces (FSSs). While conventional RF FSSs are designed based upon a planar distribution of conductive elements, this leaves the large design space of the out of plane dimension under-utilized. We investigated this design regime through the computational study of four FSS origami tessellations with conductive dipoles. The dipole patterns showed increased resonance shift with decreased separation distances, with the separation in the direction orthogonal to the dipole orientations having a more significant effect. The coupling mechanisms between dipole neighbours were evaluated by comparing surface charge densities, which revealed the gain and loss of coupling as the dipoles moved in and out of alignment via folding. Collectively, these results provide a basis of origami FSS designs for experimental study and motivates the development of computational tools to systematically predict optimal fold patterns for targeted frequency response and directionality.

Keywords: origami, frequency selective surface, tuning, radio frequency

1. INTRODUCTION

Origami, the art of paper folding, has been applied in many engineering disciplines to explore new design concepts such as self-assembled devices [1, 2] and foldable robots [3-5]. Notable examples demonstrate that origami can offer guidance to the design of spatially reconfigurable devices. Application of this design concept in radio-frequency (RF) devices is particularly relevant as the electromagnetic (EM) interactions of RF components are sensitive to geometry and relative spacing of conductive elements [6, 7].

Reconfigurability of RF devices are often attained through inclusion of lumped components; some of the emerging techniques involve integration of metamaterial-inspired designs with varactor tuning [8] and microfluidics for medium property tuning [8, 9]. While spatial re-arrangement of components leads to a dramatic expansion of the design space, such design strategies have been under-utilized for a number of reasons. Traditionally, there was not enough motivation to consider 3D designs or inclusion of morphing components due to the added complexity and manufacturing challenges. Recent development in advanced manufacturing technology such as additive and subtractive manufacturing and smart materials enables arbitrarily complex fabrications at a relatively low cost, providing new opportunities to reconsider the way we design devices. In addition, the complex relationship between geometries and RF component interactions limited the use of traditional empirical or analytical-based design approaches for 3D device designs. Powerful computational tools facilitate the performance evaluation of a device with general 3D geometry, for example, using the finite element method (FEM). Origami design concepts provide a convenient design constraint to spatial reconfiguration so that any design in consideration is physically realizable through folding.

To demonstrate the design concept, this article presents spatial reconfiguration of frequency response of a well-known system of dipole-based frequency selective surfaces (FSSs) through origami folding. The study focuses on the designs investigated in [10]; new simulations in the S-band (2-4GHz) frequency range are carried out to analyze the effect of material properties and underlying principles of resonance tuning.

Automatic Target Recognition XXVI, edited by Firooz A. Sadjadi, Abhijit Mahalanobis,
Proc. of SPIE Vol. 9844, 98440W · © 2016 SPIE · CCC code: 0277-786X/16/$18 · doi: 10.1117/12.2224160

2. FOLDABLE GEOMETRY

2.1 Rigid foldable patterns

The fold patterns evaluated in this study follow the definition of rigid foldability. The rigid foldable model assumes all facets and foldlines are perfectly rigid. Such geometric reconfiguration may be described through affine transformation [11] as illustrated in Figure 1 (a) and used to carry out the simulation of the folding process using the time derivative [12]. The necessary condition for rigid foldability of each vertex is written as

$$\mathbf{F} = R_1 R_2 \cdots R_n = \boldsymbol{I} \tag{1}$$

where R_i denotes the following transformation matrix referring to sector angle and fold rotations of line *i* and facet *i*:

$$R_i = R_{i\rho} R_{i\theta} = \begin{bmatrix} 1 & 0 & 0 \\ 0 & cos\rho_i & -sin\rho_i \\ 0 & sin\rho_i & cos\rho_i \end{bmatrix} \begin{bmatrix} cos\theta_i & -sin\theta_i & 0 \\ sin\theta_i & cos\theta_i & 0 \\ 0 & 0 & 1 \end{bmatrix} \tag{2}$$

While sector angles: $\theta's$ are fixed for each crease pattern, fold angles: $\rho's$ are state variables that determine the folded configuration, whose evolution describes the folding process. The differential form:

$$\mathbf{C}\dot{\boldsymbol{\rho}} = \mathbf{0} \tag{3}$$

is used to evolve the fold angles $\boldsymbol{\rho}$. Readers are referred to [12] for the numerical solution method of Eq. (3).

The computed fold angles are then used to access the folded configuration of a "snapshot" at an interested time. Rigid folding simulation has a relatively low computational cost, especially those that exhibit a high level of symmetry, and is well suited for computing folded geometries of known folding patterns.

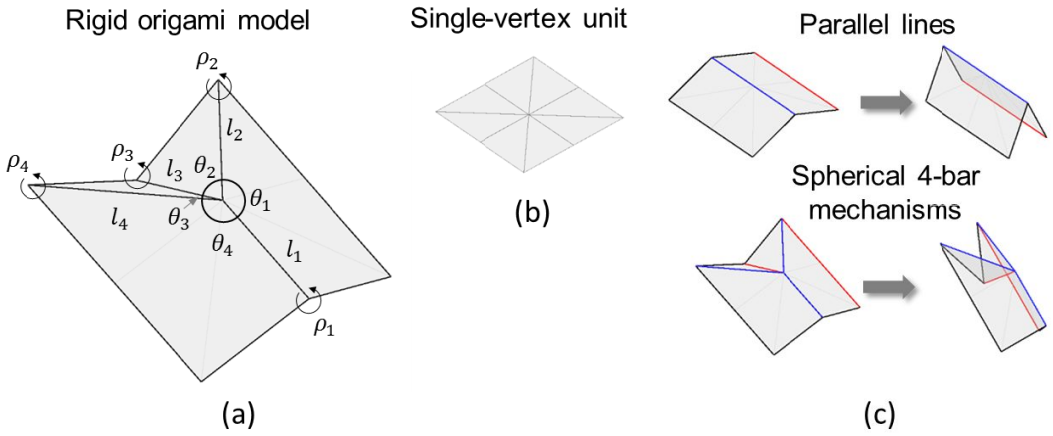

Figure 1. Representative notation and schematic of rigid origami model. (a) Definition of sector angles, θ_i, and fold angles, ρ_i, at a single vertex with four folds, and (b) 8-fold single vertex in the flat state. (c) Example folds available on 8-fold reference grid. Blue denotes "mountain" fold and red denotes "valley".

2.2 Rigid foldable tessellations

This work considers infinite FSSs analyzed using FEM with periodic conditions. Therefore, origami designs considered here are restricted to tessellations that fold and un-fold along a flat plane, without creating an overall curvature. Four tessellations shown in Figure 2 can be constructed based on the fold pattern units in Figure 1 (b). These tessellations all fold along a flat plane. For consistency across all fold patterns considered, dipoles are printed, following the geometry mapping on the single vertex unit, shown in Figure 3 (a),(b).

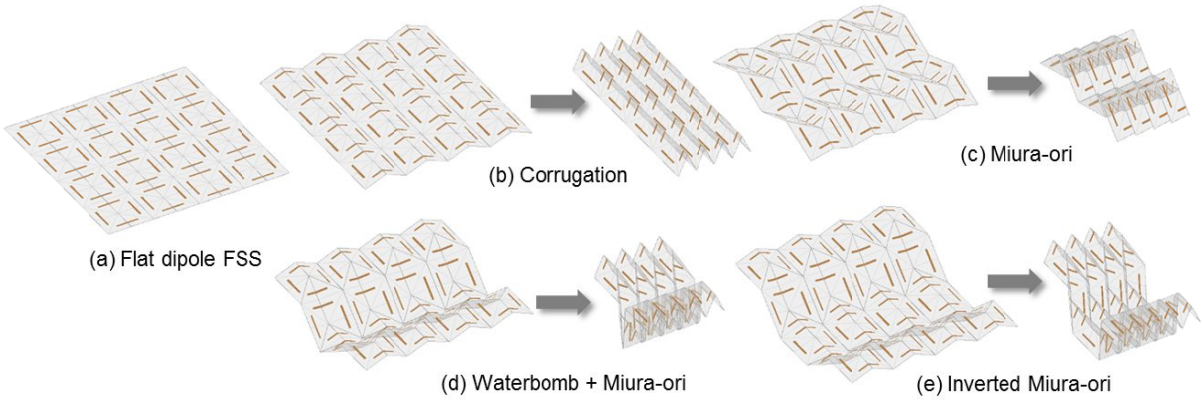

Figure 2. Dipole FSSs folded origami tessellations. a) flat dipole FSS; b) corrugated dipole FSS; c) dipole FSS folded following Miura-ori; d) dipole FSS folded following a tessellation that combines Miura-ori and waterbomb bases; e) dipole FSS folded following a tessellation that combines Miura-ori and inverted Miura-ori.

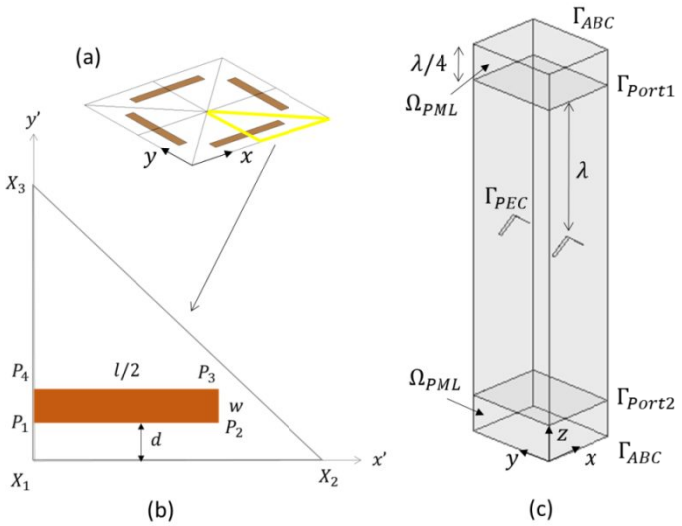

Figure 3. Schematic of conductive element layout of the FSS. (a) Dipole layout on unit cell (b) Notation and reference frame used to parameterize dipole location on unit cell, (c) FEM periodic bounding box setup in COMSOL.

3. ELECTROMAGNETIC ANALYSIS

3.1 Assumptions in the model

Dipole-based foldable FSSs operational in the S-band are considered. Their frequency responses are evaluated using finite element method in COMSOL, a commercial multiphysics FEM software. Simplified assumptions regarding the material properties of constituents in the foldable FSSs are used in order to reduce the computational cost of the EM analysis. Key assumptions involve the elimination of the effect of the dielectric substrate and the conductive loss. These assumptions are justified in this study because the dielectric substrate is assumed to be very thin compared to the relevant wavelengths with a minor effect on the FSS performance, and the elimination of the thin substrate from the model improves the computational efficiency significantly. The conductive traces are assumed to be a good conductor, for example, copper ($\sigma = 6.0 \times 10^7 S/m$) with negligible effects on the frequency response in the RF range. Results of numerical experiments, investigating the effect of these assumptions, are presented in Sec.3.3.

3.2 Analysis using FEM in COMSOL

Based on the assumptions discussed in the previous section, the EM analysis model is set up as illustrated in Figure *3* (c). The substrate is assumed to have negligible effect and is not drawn. The dipoles are drawn, for each folded configuration of interest, such that they follow the folded pattern. A dipole layout on a general single-vertex unit is shown in Figure *3* (a). The new coordinates of dipoles on folded substrate can be calculated using a geometric mapping such as one shown in Figure *3*(b). The vector Helmholtz equation is solved for the electric field, assuming time harmonic behavior. Perfectly electric conductor (PEC) BCs are used for the dipole surfaces. Absorbing boundary conditions are used at the top and the bottom boundaries to truncate the computational domain. Port boundary conditions are used to apply the excitation at a prescribed frequency, angle of incidence and polarization. Perfectly matched layers (PMLs) of quarter wavelength thickness are applied at the top and bottom to suppress artificial reflections from those boundaries. The height of the computational domain is set such that the distance between the dipoles and the port boundaries is at least a full wavelength.

Mesh density is determined relative to the wavelength λ_0 that corresponds to the highest frequency used in the frequency sweep. The conductive traces were discretized using triangular elements of the maximum size $\lambda_0/30$. The deviation in the resonant frequency when using the maximum size $\lambda_0/15$ is 1.5%. The computational accuracy is most sensitive to the mesh on the conductive traces. The rest of the model is discretized according to the conductive trace mesh, with the size of the tetrahedral elements growing, away from the dipoles, up to the maximum dimension of $\lambda_0/6$.

To improve the computational efficiency, only the dipoles aligned with the excitation are drawn and meshed in COMSOL. For instance, when the FSS is excited with plane waves with the electric field along the x-axis, only the two parallel dipoles along the x-axis are drawn. From the principles of FSS design [13] and previous numerical experiments [10], the dipoles aligned with the input electric field are excited with a current flow at the resonant frequency, while the dipoles orthogonal to the input electric field experience no induced current. A numerical test was conducted to confirm that the orthogonal dipoles do not affect the simulation and can be removed from the model without affecting the analysis.

3.3 Effects of material properties

Numerical experiments are conducted to investigate the material assumptions of the model, as discussed in Sec. 3.1 by inserting published versus idealized material properties of the dielectric substrate and finite conductivity for a flat dipole FSS. Figure 4 shows a summary of these studies. The black solid line refers to the frequency response of the transmission coefficient for a dipole FSS using no material properties, i.e., no substrate with PEC for the dipole. A strong resonance at 3.42GHz is observed. Changing the dipole surface to have the conductivity of copper ($\sigma = 6.0 \times 10^7 S/m$) has virtually no effect. Inclusion of a dielectric substrate with dielectric constant $\varepsilon_r = 2.2$ and thickness 1mm moves the resonance down to 3.21GHz, by 6%. Inclusion of a thin dielectric substrate with 0.5mm thickness leads to a 4% downward shift in resonance. Use of a degraded conductor reduces the Q-factor, in an extreme case ($\sigma = 1.0 \times 10^4 S/m$), removing the resonance.

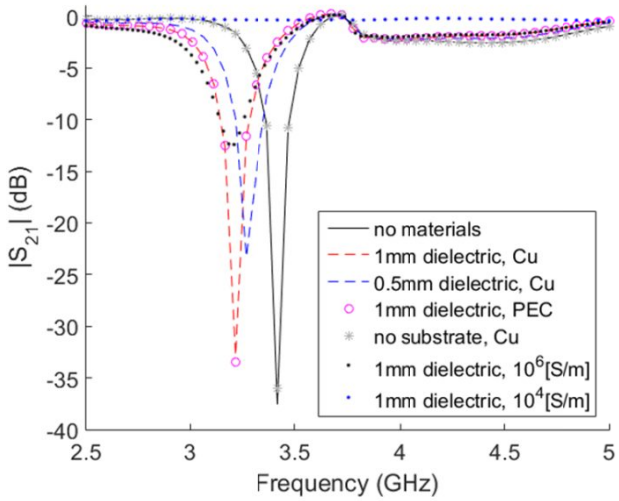

Figure 4. Comparison of frequency response of the transmission coefficient

4. RESULTS

4.1 Dipoles on tessellations

Frequency responses of dipoles following folded substrates, excited by a plane wave with the electric field aligned with the x-axis, are shown in Figure *5*. Fictitious time t indicates how far the substrate is folded. The corresponding changes in the projected x-length, ΔL_x, are summarized in Table 1.

Table 1. Fold evolution parametrized by "time" t and the corresponding change in the projected x-length ΔL_x

t: "time"	1	10	20	30	40	50
ΔL_x: change in the x-length	0	-1.7%	-7.7%	-19.1%	-36.5%	-59.5%

In all of the fold patterns tested, the resonant frequency tends to shift upward, following the changes in the periodicity and dipole re-orientation, as the substrate is folded. Folding introduces no significant difference in the strength of the resonance in corrugation and Miura-ori until the sheet is very much folded. The frequency response is more complex in the other two fold patterns, involving changes in the strength of resonance and multiple resonances for strongly folded structures.

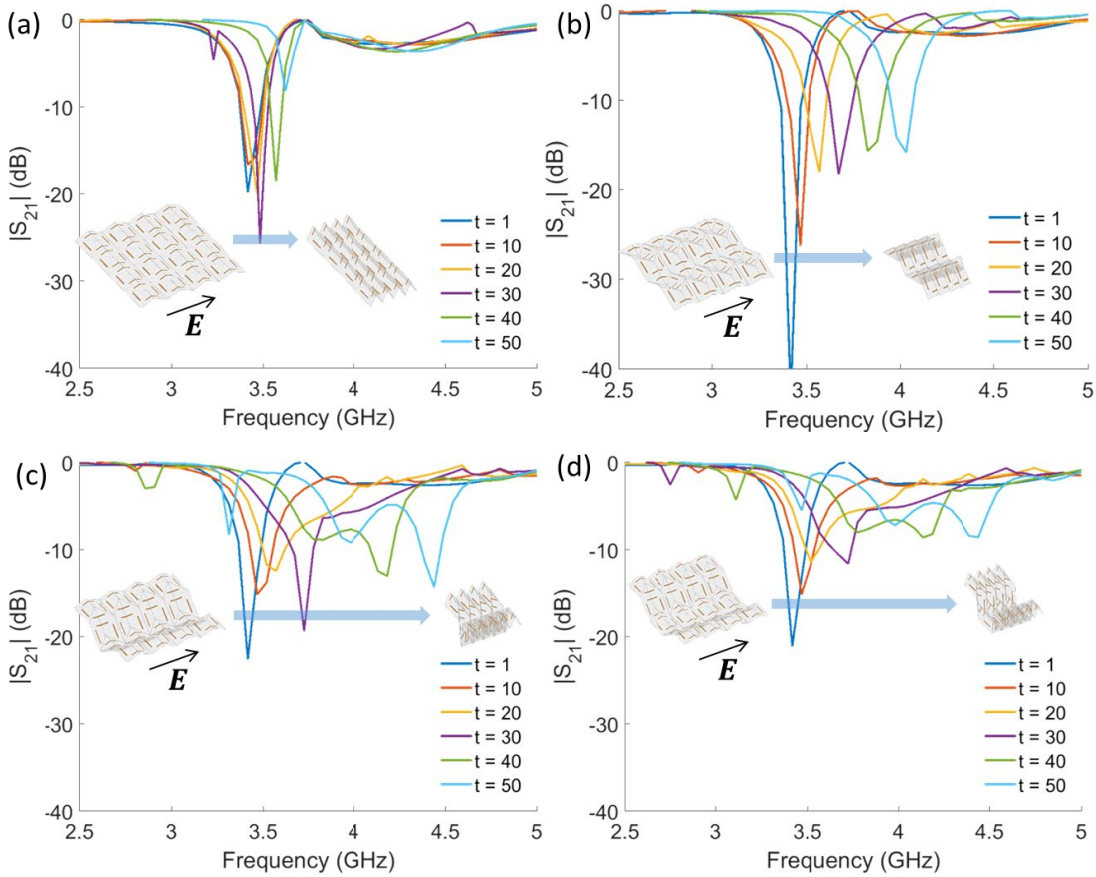

Figure 5. Frequency response of dipoles with the horizontal polarization. Excited dipoles are across the corrugation direction, creating bends in dipoles. a) corrugation; b) Miura-ori; c) Miura-ori and waterbomb base; d) inverted Miura-ori.

Frequency response of dipoles following folded substrates, excited by a plane wave with the electric field aligned with the y-axis, are shown in Figure *6*. One of the notable differences from the frequency responses of the other polarization is that the resonance becomes weaker as the sheet is folded further, following Miura-ori. This is because the folding creates misalignment in the dipole orientations with respect to each other, creating an effect similar to polarization misalignment, relative to the input electric field (see Figure 7). By comparison, in the horizontal polarization case for corrugation and Miura-ori, each dipole is folded, but the alignment to its neighbors aligns with the incident electric field, leading to only a minor effect on the quality factor.

Another interesting phenomenon is seen in Figure 6 (c),(d). The misalignment of the dipoles and the incident electric field leads to a degraded quality factor, as before, as the sheet is folded from the t =1 state towards the t =10 state. At the t =20 state, the resonance is almost gone, and the location of the minimum is shifted slightly towards a lower frequency. At the t =30 state, the response is back to dipoles resonating at a higher frequency. The surface current density plot in Figure 8 (a) reveals that folding induces dipole orientation reconfigurations such that, for a certain folding range, the combination of dipole misalignment and their separation creates a performance gap. At the t =20 state in Figure 8 (a) center, the four dipoles in the middle experience no current flow, leaving the outer dipoles to bridge between a large gap, leading to a weak response. As the sheet is folded further, the slanted dipoles in the middle become closer together, leading to a current flow.

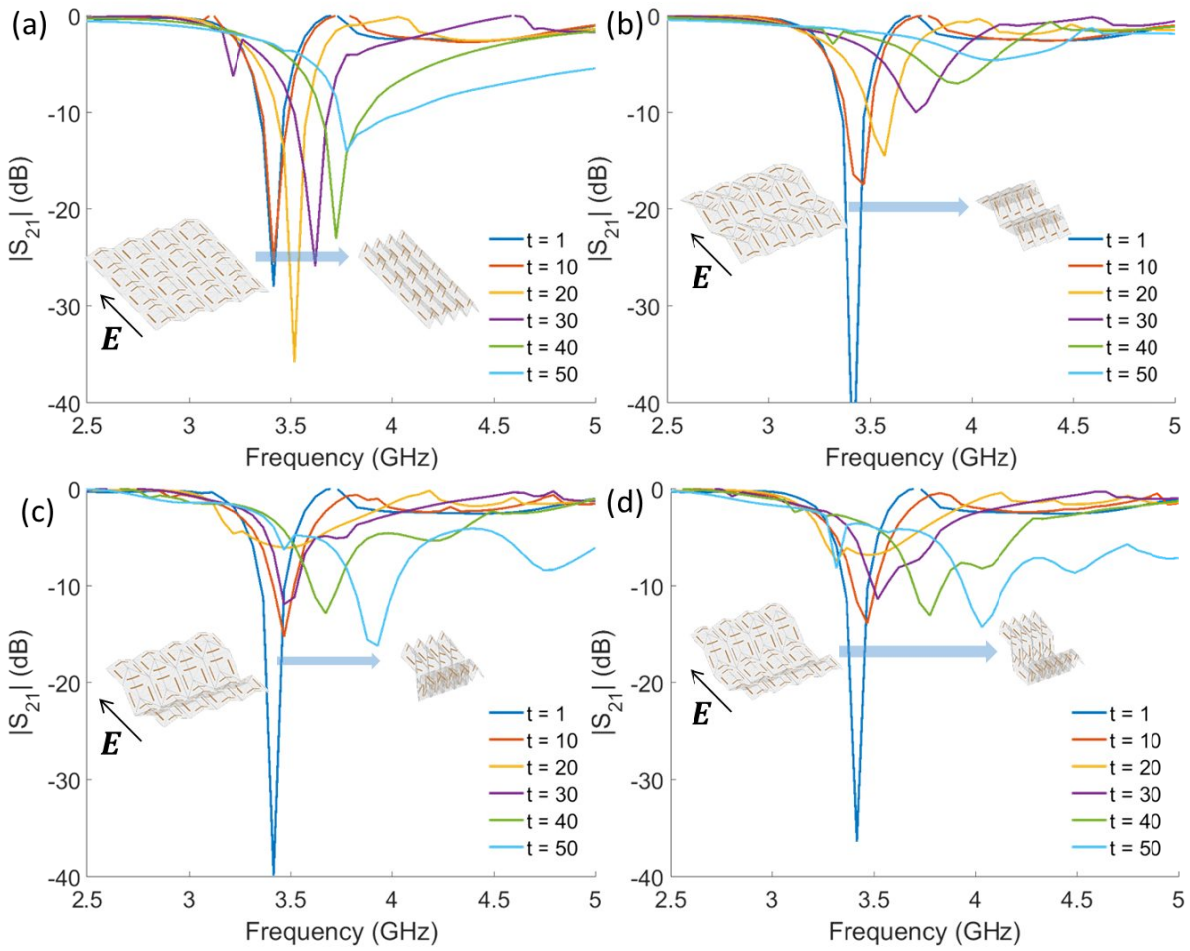

Figure 6. Frequency response of dipoles with the vertial polarization. Excited dipoles are parallel to the corrugation direction; no bend in dipoles. a) corrugation; b) Miura-ori; c) Miura-ori and waterbomb base; d) inverted Miura-ori.

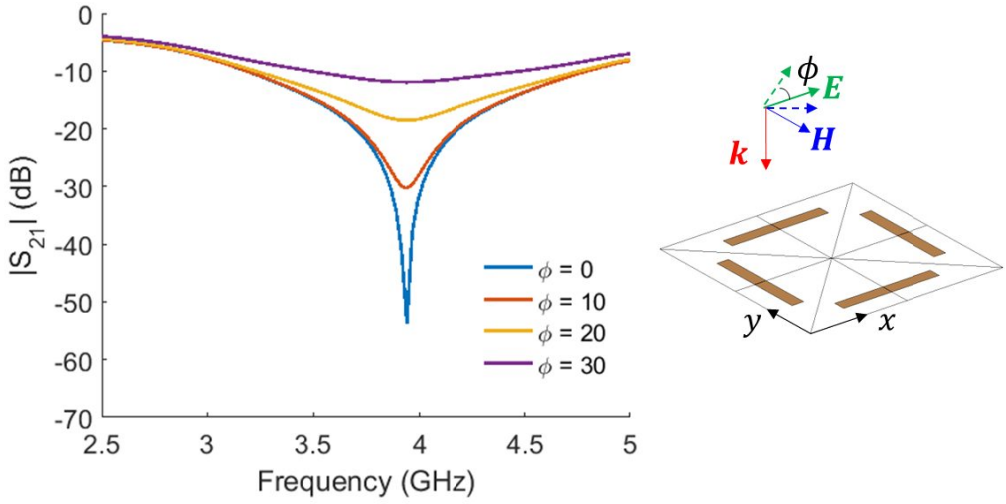

Figure 7. Degraded quality factors, as the polarization becomes skewed from the dipole alignment.

Proc. of SPIE Vol. 9844 98440W-7

The surface current plot can be used to investigate the phenomenon leading to two dips in the transmission for Miura-ori and waterbomb base and inverted Miura-ori patterns, with the horizontal polarization. In Figure 8 (b), the dip at the lower frequency corresponds to outer dipoles experiencing stronger current, while the dip at the higher frequency corresponds to inner dipoles having a stronger current flow, creating two different modes of operation. A careful re-design to merge those to dips together could lead to a wide stop band.

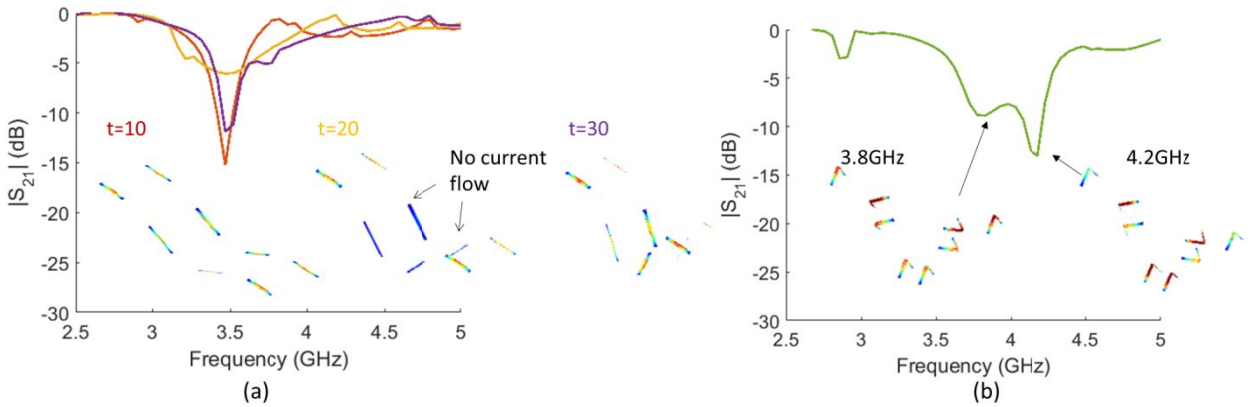

Figure 8. Surface current density at the resonance of dipoles folded following Miura-ori and waterbomb base pattern. a) the four middle dipoles experience no current flow at the $t = 20$ folded state with the vertical polarization, leading to a weak response; b) two different modes of operation, leading to two dips in the transmission coefficient at the $t = 40$ folded state with the horizontal polarization.

4.2 Performance reconfiguration trends

The trends in the resonance shifting are summarized in Figure 9. As discussed in the previous section, changes in the periodicity span leads to shifts in resonant frequency. The trend shown in Figure 9 (a) and parametric studies on the effect of the periodicity span on the resonant frequency (see Figure 10) indicate that, in case of the horizontal polarization, shortening the periodicity span in the direction orthogonal to the dipole/electric field alignment has the dominant effect. The parametric studies show that the decrease in the periodicity span in the orthogonal, L_y direction has a monotonic effect of increasing the resonant frequency. The trend curves in Figure 9 (a) exhibits a larger resonant frequency increase in fold patterns that produce a larger decrease in L_y. The increase in the resonant frequency is enhanced due to bends created along dipoles, causing an effect similar to changing the angle of incidence.

The trend seen in Figure 9 (b) is consistent with the discussions above. The periodicity span in the direction perpendicular to the dipoles aligned with the electric field changes at the same rate for all fold patterns, resulting in a similar rate of increase of resonant frequency. The non-monotonic behavior observed in Figure 9 (b) for the Miura-ori and waterbomb base and inverted Miura-ori pattern is due to the dipole misalignment observed in Figure 8 (a).

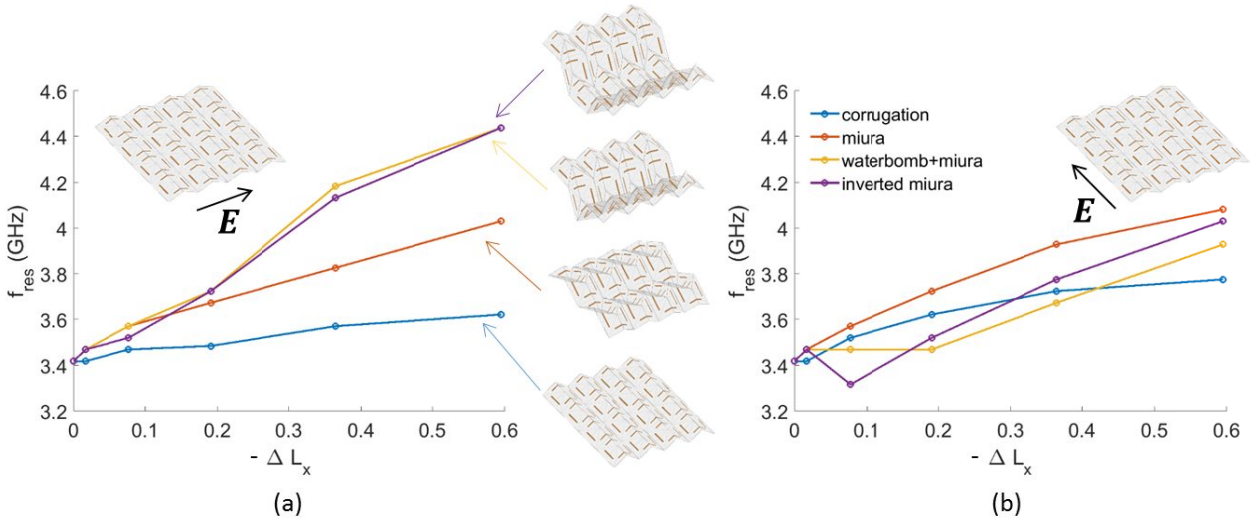

Figure 9. The resonance shift trends of dipoles following four different origami tessellations. a) horizontal polarization; b) vertical polarization.

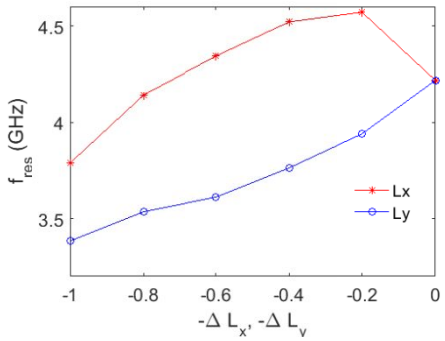

Figure 10. Parametric study on dipole FSS resonance for varying periodicity span. Dipoles are oriented along the x-axis. The right side of the plot indicates a smaller periodicity span, mimicking "later" folding steps.

5. CONCLUSION

Dipole FSS was folded in four known origami tessellations and simulated for the S-band operation. The general trend of the resonance frequency increase was observed across different configurations, due to changes in the periodicity span. The dominant effect seems to be the periodicity in the direction orthogonal to the dipole aligned with the electric field. Combination of other phenomena due to the complex geometric reconfigurations are observed, including the degraded quality factor for fold patterns that result in dipole misalignment, and multiple modes of operation produced to several non-identical lines of dipoles caused by some folding patterns breaking the symmetry.

The origami tessellations and dipole patterns evaluated in this study demonstrate the potential of spatial reconfiguration for tuning the resonance frequency of a FSS. The study also provided new insights into coupling mechanisms for 2D EM resonators embedded in a 3D space, which has implications for other EM applications. Further design tools are needed to identify new fold patterns and folding paths that enhance this tuning capability, while satisfying additional constraints. Engineering constraints, such as actuator placement, attachment points within a specific device, and retaining displacement precision while in operation will be important considerations for a foldable FSS to achieve practical utility. Together, this computational study predicts a set of FSS designs with measurable resonance shifts and motivates the further computational and experimental investigation of an origami-based approach to FSS tuning.

6. ACKNOWLEDGMENTS

This research is supported under the Air Force Office of Scientific Research funding, LRIR 13RQ02COR.

REFERENCES

[1] Gracias, D. H., Kavthekar, V. , Love, J. C., Paul, K. E., and Whitesides, G. M., "Fabrication of micrometer-scale, patterned polyhedra by self-assembly," *Advanced Materials,* vol. 14, p. 235, 2002.

[2] Kuribayashi-Shigetomi, K., Onoe, H., and Takeuchi, S., "Cell origami: self-folding of three-dimensional cell-laden microstructures driven by cell traction force," *PloS one,* vol. 7, p. e51085, 2012.

[3] Onal, C. D., Wood, R. J. and Rus, D., "Towards printable robotics: Origami-inspired planar fabrication of three-dimensional mechanisms," in *Robotics and Automation (ICRA), 2011 IEEE International Conference on*, 2011, pp. 4608-4613.

[4] Miyashita, S., Guitron, S., Ludersdorfer, M., Sung, C. R., and Rus, D., "An untethered miniature origami robot that self-folds, walks, swims, and degrades," in *Robotics and Automation (ICRA), 2015 IEEE International Conference on*, 2015, pp. 1490-1496.

[5] Lee, D.-Y., Jung, G.-P., Sin, M.-K. Ahn, S.-H., and Cho, K.-J., "Deformable wheel robot based on origami structure," in *Robotics and Automation (ICRA), 2013 IEEE International Conference on*, 2013, pp. 5612-5617.

[6] Fuchi, K., Tang, J., Crowgey, B., Diaz, A. R., Rothwell, E. J., and Ouedraogo, R. O., "Origami tunable frequency selective surfaces," *Antennas and Wireless Propagation Letters, IEEE,* vol. 11, pp. 473-475, 2012.

[7] Fuchi, K., Diaz, A. R., Rothwell, E. J., Ouedraogo, R. O. and Tang, J., "An origami tunable metamaterial," *Journal of Applied Physics,* vol. 111, p. 084905, 2012.

[8] Tang, J., Ouedraogo, R. O., Rothwell, E. J., Diaz, A. R., and Fuchi, K., "A continuously tunable miniaturized patch antenna," *Antennas and Wireless Propagation Letters, IEEE,* vol. 13, pp. 1080-1083, 2014.

[9] Barrera, J. D.and Huff, G. H., "A fluidic loading mechanism in a polarization reconfigurable antenna with a comparison to solid state approaches," *Antennas and Propagation, IEEE Transactions on,* vol. 62, pp. 4008-4014, 2014.

[10] Fuchi, K., Buskohl, P.R., Reich, G., Vaia, R. and Joo, J. , "Resonance Tuning of RF Devices through Origami Folding," in *ICCM: 20th International Conference on Composite Materials*, Copenhagen, 2015.

[11] belcastro, s.-m. and Hull, T. C., "Modelling the folding of paper into three dimensions using affine transformations," *Linear Algebra and its applications,* vol. 348, pp. 273-282, 2002.

[12] Tachi, T., "Simulation of rigid origami," *Origami,* vol. 4, pp. 175-187, 2009.

[13] Munk, B. A. , *Frequency selective surfaces: theory and design*: John Wiley & Sons, 2005.